Computers, Materials & Continua CMC, vol.63, no.3, pp.1533-1543, 2020

High Resolution SAR Image Algorithm with Sample Length Constraints for the Range Direction

Zhenli Wang[1, *], Qun Wang[1], Fujuan Li[1] and Shuai Wang[2]

Abstract: The traditional Range Doppler (RD) algorithm is unable to meet practical needs owing to the limit of resolution. The order of fractional Fourier Transform (FrFT) and the length of sampling signals affect SAR imaging performance when FrFT is applied to RD algorithm. To overcome the above shortcomings, the purpose of this paper is to propose a high-resolution SAR image algorithm by using the optimal order of FrFT and the sample length constraints for the range direction. The expression of the optimal order of SAR range signals via FrFT is deduced in detail. The initial sample length and its constraints are proposed to obtain the best sample length of SAR range signals. Experimental results demonstrate that, when the range sampling-length changes in a certain interval, the best sampling-length will be obtained, which the best values of the range resolution, PSLR and ISLR, will be derived respectively. Compared with traditional RD algorithm, the main-lobe width of the peak-point target of the proposed algorithm is narrow in the range direction. While the peak amplitude of the first side-lobe is reduced significantly, those of other side-lobes also drop in various degrees.

Keywords: Fractional Fourier transform, synthetic aperture radar, range doppler algorithm, image quality assessment.

1 Introduction

At present, synthetic aperture radar (SAR) imaging [Sourabh and Umesh (2020); Shahzad, Liam, Marina et al. (2019); Hajar and Bijan (2019); Nizar and Stéphane (2019); Qiu, Zhou and Fu (2020)] reconnaissance has attracted the attention of all countries in the world, and has become a technology that shows fierce competition and rapid development. As an effective air-to-ground observation tool, SAR imaging reconnaissance can provide long-distance and all-weather detection activities, and plays an increasingly important role in modern police operations [He, Yu, Xu et al. (2019)]. RD algorithm is a classical method for SAR imaging processing thanks to its easy operability and high computational efficiency [Smith (1991)]. However, its strength is greatly compromised by its weakness: the quality of the acquired images is very low, hence

[1] Department of Computer Information and Network Security, Jiangsu Police Institute, Nanjing, 210031, China.

[2] Department of Radiology and BRIC, University of North Carolina at Chapel Hill, North Carolina, 27599, USA.

[*]Corresponding Author: Zhenli Wang. Email: dongwen3619@sina.com.

Received: 16 January 2020; Accepted: 28 February 2020.

greatly reduces the applicability of the algorithm. The Secondary Range Compression (SRC), a modified algorithm, is able to improve the imaging accuracy of SAR, but its dependence on the azimuth frequency [Cumming and Wong (2005)] becomes yet another problem that is difficult to resolve.

The application of FrFT to SAR imaging processing has been a focus of research in recent years, and researchers are particularly interested in the fractional orders. Two-dimensional peak spectrum search [Fouts and Pace (2002)] in fractional Fourier domain is proposed to determine the optimal transform order of FrFT for Linear Frequency Modulation (LFM) parameter estimation. This method has very good stability, but a tremendous amount of calculation is required, and the precision of parameter estimation is reduced due to the limited amount of data samples. By using geometric transformation relationship, the optimal order of FrFT for LFM signals [Capus and Brown (2003)] can be obtained, but the corresponding FrFT cannot replace the Fourier Transform (FT) in traditional RD algorithm to achieve signal reconstruction. The literature [Chen, Zhao, Chen et al. (2014)] measures the frequency modulation of SAR echo signals by way of local optimal processing and calculates the optimal order of FrFT, which is effective in improving the imaging performance of missile-borne SAR according to its experimental results, but it is not universally applicable. In the reported research results of applying FrFT to SAR imaging [Ramona, Nicolas, Grégoire et al. (2016); El-Mashed, Zahran, Dessouky et al. (2013); Wang and Jiang (2018)], a good solution has not been found to replace traditional Fourier Transform to achieve higher image resolution. In an attempt to resolve the application problem of FrFT and the sample length constraints for the range direction, this paper starts with the order analysis of range signal transform, then establishes a high-resolution SAR imaging algorithm based on the optimal order of FrFT and the sample length constraints for the range direction, and finally concludes with a presentation of experimental results and an analysis of the point-target imaging of airborne side-looking SAR and the measured data of the space-borne RADARSAT-1.

2 Order analysis of range signal transform

It is assumed that the slant distance between P′ and T is $R(t)$, where t is a slow time variable when the SAR platform moves to any position P′ on the flight path, point T is located at the center of SAR imaging swath. The LFM signals emitted by SAR at any position P′ is shown in Eq. (1).

$$s_r(\tau) = \mathrm{rect}\left(\frac{\tau}{T_P}\right)\exp\left(\mathrm{j}2\pi f_c\tau + \mathrm{j}\pi\kappa_r\tau^2\right) \tag{1}$$

where τ is the fast time variable, T_p is the pulse width, f_c is the carrier frequency, κ_r is the modulation frequency of SAR echo signals, c is the light speed and $\mathrm{rect}(\cdot)$ is the rectangular window function.

The fractional Fourier transform of the continuous-time signal $f(x)$ is defined as

$$F_\alpha\left[f(u)\right] = \int_{-\infty}^{\infty} K_\alpha(u,x) f(x)dx \tag{2}$$

where $K_\alpha(u,x)$ is the kernel function of FrFT as shown in Eq. (3), α is the rotation angle

and $\alpha = -\mu \times \pi/2$, μ is the order of FrFT.

$$K_\alpha(u,x) = A_\alpha \cdot \exp\left\{ j\pi \left[\left(x^2 + u^2\right)\cot\alpha - 2ux\csc\alpha \right] \right\} \tag{3}$$

where $A_\alpha = \sqrt{1 - \mathrm{j}\cot\alpha}$, and $\alpha \neq n\pi$. If $\alpha = 2n\pi$, $K_\alpha(u,x) = \delta(u-x)$, and if $\alpha = (2n+1)\pi$, $K_\alpha(u,x) = \delta(u+x)$. Considering the time delay, Eq. (2) is substituted for the SAR range signals in Eq. (1).

$$F_\alpha\left[S_r(u)\right] = \int K_\alpha(u,\tau)\,\mathrm{rect}\left[\frac{\tau - \dfrac{2R(t)}{c}}{T_P}\right] \times \exp\left[\mathrm{j}2\pi f_c\left(\tau - \frac{2R(t)}{c}\right) + \mathrm{j}\pi\kappa_r\left(\tau - \frac{2R(t)}{c}\right)^2 \right] d\tau \tag{4}$$

To simplify the calculation, the following settings are substituted into Eq. (4) without producing adverse effect on the optimal order analysis of FrFT, where $f_c = 0$, $R(t) = 0$, and $W_r(\tau) = \mathrm{rect}(\tau/T_P)$.

$$\begin{aligned} F_\alpha\left[s_r(u)\right] &= \int_{-\infty}^{\infty} K_\alpha(u,\tau) W_r(\tau) \exp\left(\mathrm{j}\pi\kappa_r\tau^2\right) d\tau \\ &= A_\alpha \int_{-\infty}^{\infty} W_r(\tau) \times \exp\left\{ \mathrm{j}\pi \left[\left(\tau^2 + u^2\right)\cot\alpha - 2u\tau\csc\alpha + \kappa_r\tau^2 \right] \right\} d\tau \end{aligned} \tag{5}$$

Assume $U(\tau) = W_r(\tau)$, then $V(\tau) = \exp\left\{ \mathrm{j}\pi \left[\left(\tau^2 + u^2\right)\cot\alpha - 2u\tau\csc\alpha + \kappa_r\tau^2 \right] \right\}$. According to the Principle of Stationary Phase, Taylor formula and Fresnel integral [Wang and Wang (2020)], the following equation can be obtained

$$F_\alpha\left[s_r(u)\right] = \frac{A_\alpha W_r\left(\dfrac{u\csc\alpha}{\kappa_r + \cot\alpha}\right)}{\sqrt{\kappa_r + \cot\alpha}} \times \exp\left[\mathrm{j}\pi u^2 \left(\cot\alpha - \frac{\csc^2\alpha}{\kappa_r + \cot\alpha} \right) + \frac{\pi}{4} \right] \tag{6}$$

Assume that the sampling-length of the SAR echo signals in the range direction is N_r, the sample frequency is F_r, the modulation frequency after the dimensional normalization of the range signal [Zhao, Deng and Tao (2005)] is κ_r', the rotation angle is α', substitute them into Eq. (6) and get

$$F_{\alpha'}\left[s_r(u)\right] = \frac{A_{\alpha'} W_r\left(\dfrac{u\csc\alpha'}{\kappa_r' + \cot\alpha'}\right) \exp\left(\mathrm{j}\dfrac{\pi}{4}\right)}{\sqrt{\kappa_r' + \cot\alpha'}} \times \exp\left[\mathrm{j}\pi u^2 \left(\cot\alpha' - \frac{\csc^2\alpha'}{\kappa_r' + \cot\alpha'} \right) \right] \tag{7}$$

According to Eq. (7), if the fractional energy spectrum $F_{\alpha'}\left[s_r(u)\right]$ is highly focused on a certain fractional Fourier transform domain axis at the rotation angle of α', then $\kappa_r' + \cot\alpha' = 0$ is certainly satisfied, and at this moment $F_{\alpha'}\left[s_r(u)\right]$ is an impulse

function. Because $\kappa_r' = \kappa_r N_r / F_r^2$, $\alpha' = \frac{\pi}{2}\mu'$, $\alpha' = \alpha$, the optimal order of the SAR echo signals in the range direction at the time of fractional Fourier transform can be obtained

$$\mu_{\text{opt}} = \mu' = \frac{2}{\pi}\arctan\left(-\frac{F_r^2}{\kappa_r N_r}\right) \tag{8}$$

where arctan(.) is the inverse tangent function. For an actual given echo signals of SAR, the range frequency κ_r, the sampling-length N_r and the sampling frequency F_r are all known, so it is easy to directly calculate the corresponding optimal order μ_{opt} according to Eq. (8).

3 Sample length constraints for the range direction

Any fractional order of FrFT corresponds to a time-frequency rotation angle. If it is the optimal order, the energy spectrum of FrFT under the corresponding time-frequency rotation angle is an impulse function as mentioned earlier. Therefore, the optimal order of FrFT and the optimal rotation angle are the unique corresponding relations. Theoretically, the optimal order of fractional Fourier transform can be obtained as long as the length of range samples meets the basic requirements of SAR imaging. However, the sample length satisfying the above conditions has certain uncertainty, which does not necessarily bring about the optimal SAR imaging performance. In order to solve this problem, we present a method to calculate the best sample length of range signals.

Let the initial sample length of range signals be Nr_0, as shown in Eq. (9):

$$Nr_0 = \text{INT}[\gamma \cdot T_P \cdot F_r] \tag{9}$$

where INT[·] is the Rounding Function, γ is the variable constant, and $\gamma = 1.2$ is recommended for Airborne SAR imaging or spaceborne SAR imaging.

Take the initial sample length Nr_0 as the center, change (increase or decrease) the sample length within a certain interval, observe the SAR image resolution, and determine the best sample length according to the constraints, as shown in Eq. (10):

$$N_{r_{\text{opt}}} = \underset{|\text{PSLR}(N_r)|\to\max,|\text{ISLR}(N_r)|\to\max}{\text{argmin}}[\rho_r(N_r)] \tag{10}$$

where argmin[·] represents the variable value when the objective function $[\rho_r(N_r)]$ is taken as the minimum value, Nr_{opt} represents the optimal sample length in the range direction, which enables the range resolution ρ_r to reach the minimum value. PSLR(N_r) and ISLR(N_r) represent the corresponding PSLR (Peak Side Lobe Ratio) and ISLR (Integrated Side lobe Ratio) values respectively, when N_r changes. Eq. (10) shows that the maximum values of $|\text{PSLR}|$ and $|\text{ISLR}|$ can be obtained as much as possible when seeking the minimal range resolution ρ_r, where $|\cdot|$ is the absolute value function.

4 High resolution SAR imaging algorithm in the range direction

For SAR raw signals, especially the measured data, the rotation angles in time-frequency domain corresponding to the optimal order μ_{opt} in range direction is usually in the first quadrant of time-frequency plane, and the smaller rotation angle will reduce the focusing effect of the signals. The corresponding time-frequency angles can be rotated $\pi/2$, and the optimal order in the range direction should be changed to $1-\mu_{\text{opt}}$ (see Fig. 1).

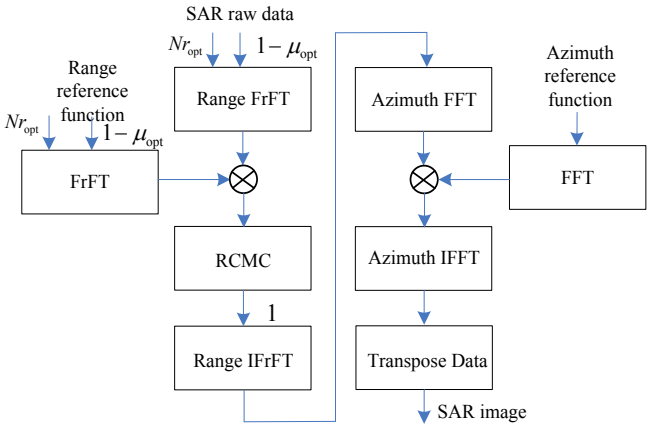

Figure 1: Construction illustrations of the proposed algorithm

The proposed algorithm in this paper can be quickly performed according to Fig. 1 in applications. Firstly, the optimal order in range direction can be easily computed by using the known imaging parameters of SAR and the optimal sample length Nr_{opt}. Secondly, the SAR range signals and range reference function are both transformed by a Fractional Fourier Transform (FrFT) to complete range pulse compression and range cell migration correction, and then the range signals are reconstructed by an Inverse Fractional Fourier Transform (IFrFT). Finally, the SAR azimuth signal and its compression reference function are both transformed by a Fast Fourier Transform (FFT) to complete azimuth pulse compression based on the range signal processing, and then the azimuth signals are reconstructed by IFFT. The calculational methods of FrFT and IFrFT in the range direction can both be effectively performed by using FFT. Theoretically, the proposed and traditional RD algorithms have the same amount of computation. The proposed algorithm becomes the traditional RD algorithm when μ_{opt} equals 0.

5 Experimental results and analysis

Taking the point-target imaging of airborne side-looking SAR as an example, the simulation parameters of airborne SAR imaging are set to T_P=5μs, F_r=120 MHz. According to the airborne SAR imaging simulation parameters, the simulation analysis is carried out with the proposed algorithm using Kaiser window function as an example. By adopting the set parameters and Eq. (9), the initial value of the range sampling-length N_{r_0} becomes 1152. With

the sampling value N_{r_0}=1152 as the reference center, the range sampling-length is extended from 800 to 1600, and the step is 2. Observe the impact of sampling-length on SAR imaging performance (see Fig. 2). The fitting curves of the range resolution ρ_r, PSLR and ISLR are all fitted by least square fitting (polynomial coefficient value is 6). It can be seen from the fitting curves in Figs 2 (a) and (b) when the range sampling-length changes from 800 to 1600, there is the best sampling-length, which enables the range resolution ρ_r, PSLR and ISLR to obtain the best values respectively, and the change trend of the latter two curves is basically the same. Taking the range resolution ρ_r as the measurement standard, the optimal sampling-length in the distance direction is 1172, and the corresponding optimal order is 1.5882. Using the proposed algorithm, the range resolution ρ_r, PSLR and ISLR are 0.85 m, -22.90 dB and -20.79 dB, respectively. At this time, the range resolution ρ_r, PSLR and ISLR of the traditional RD algorithm are 1.11 m, -13.29 dB and -10.19 dB, respectively. Fig. 3 shows the contours of the interpolated point-target by the two algorithms. Fig. 4 shows the profile images of the corresponding point-target in Fig. 3. Compared with the traditional RD algorithm, the main-lobe width of point-target in the proposed algorithm becomes narrower in the range direction, the peak amplitude of the first side-lobe decreases significantly, and those of the other side-lobes also decreases in various degrees (see Figs. 3 and 4).

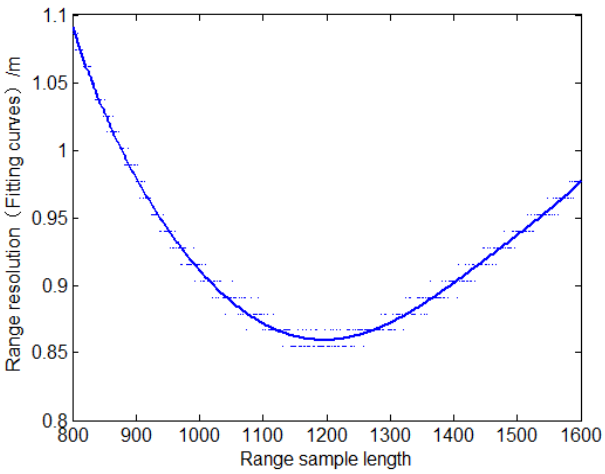

(a)

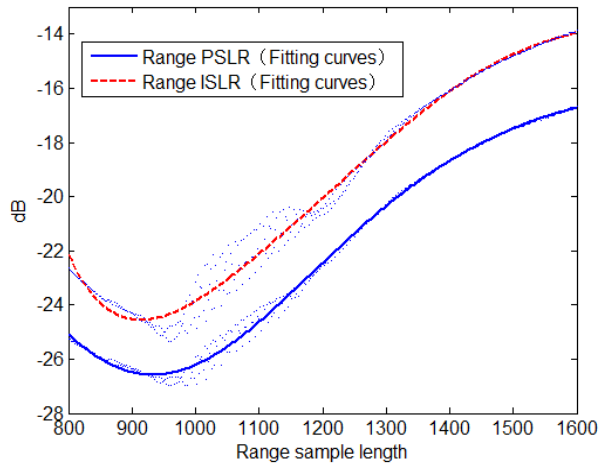

(b)

Figure 2: The influence of the range sample length on SAR imaging performance: (a) The influence of the range sampling-length on range resolution; (b) The influence of the range sampling-length on PSLR and ISLR

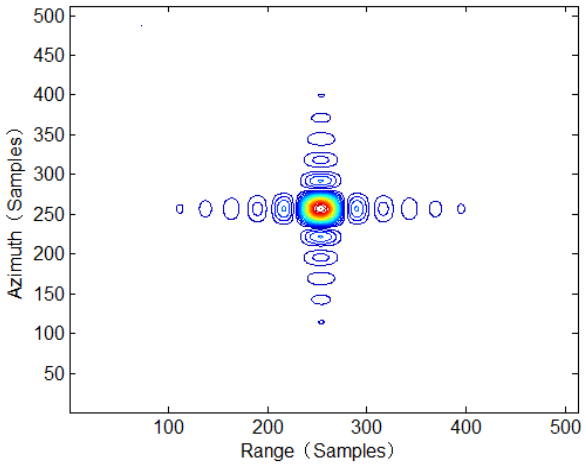

(a)

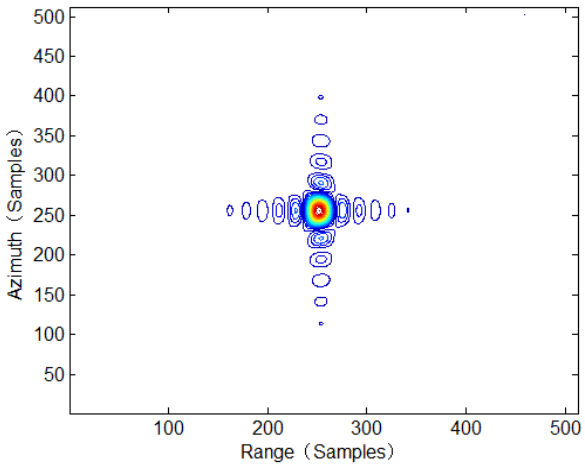

(b)

Figure 3: The contours of the interpolated peak-point target: (a) traditional RD algorithm; (b) the proposed algorithm

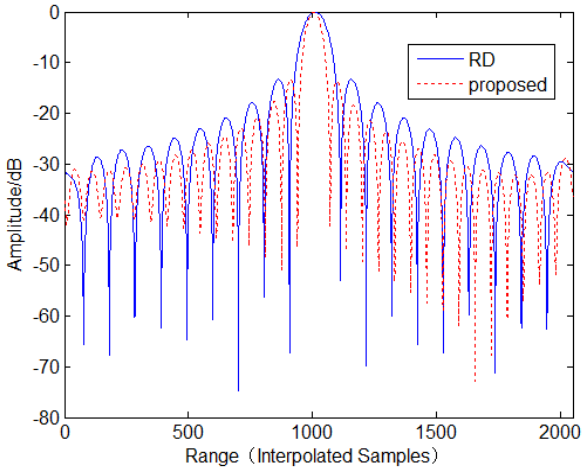

Figure 4: The profile images of the interpolated peak-point target

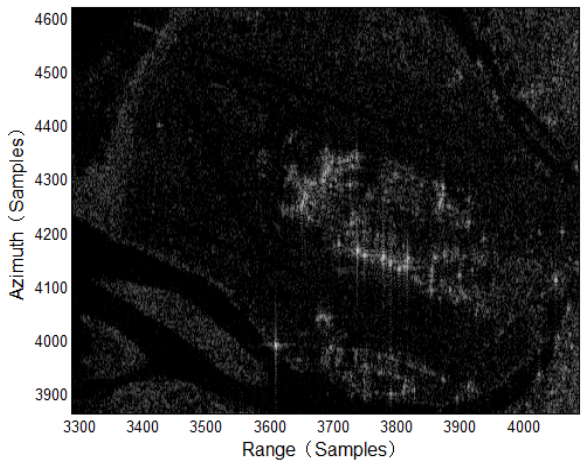

(a)

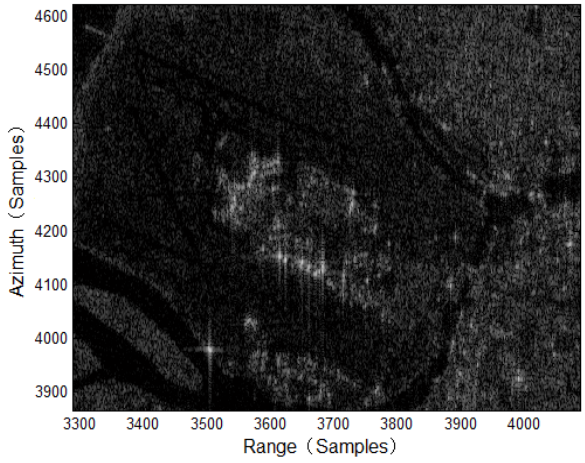

(b)

Figure 5: SAR images of measured data: (a) traditional RD algorithm; (b) the proposed algorithm

Fig. 5 shows the imaging results based on the measured data from the spaceborne SAR, the ground objects are from Canada RADARSAT-1 Vancouver scene (intercept) derived from fine mode. The imaging results in Fig. 5 show that compared with the traditional RD algorithm, the SAR image obtained by the proposed algorithm features high resolution in the range direction. On the obtained images, airport link and taxiway are clearly visible. The airborne SAR simulation data and the spaceborne SAR measurement data imaging experiments show that the proposed algorithm can achieve better SAR imaging resolution than the traditional RD algorithm in the range direction.

6 Conclusion

In this paper, a high-resolution SAR imaging algorithm is established via the optimal order of FrFT and the sample length constraints for the range direction. As far as the point-target imaging of airborne side-looking SAR and the measured data of the space-borne RADARSAT-1 are concerned, the assessed results demonstrate that the proposed algorithm performs much better than traditional RD algorithm in the range direction. The proposed algorithm in this paper has a wide application prospect in SAR imaging reconnaissance. With the continuous breakthrough and development of key SAR technology, the realization of super-high resolution, multi satellite constellation and miniaturized SAR imaging technology in the future will enable SAR reconnaissance satellite to obtain considerable development in computer vision image processing.

Acknowledgement: This work is supported by the 13th Five-Year Plan for Jiangsu Education Science (D/2020/01/22), JSPIGKZ and Natural Science Research Projects of Colleges and Universities in Jiangsu Province (19KJB510022)

Conflicts of Interest: The authors declare that they have no conflicts of interest to report regarding the present study.

References

Capus, C.; Brown, K. (2003): Short-time fractional Fourier methods for the time-frequency representation of chirp signals. *Journal of the Acoustical Society of America*, vol. 113, no. 6, pp. 3253-3263.

Chen, Y.; Zhao, H. C.; Chen, S.; Zhang, S. N. (2014): An improved focusing algorithm for missile-borne SAR with high squint. *Applied Mechanics and Materials*, vol. 608-609, pp. 761-765.

Cumming, I. G.; Wong, F. H. (2005): *Digital Processing of Synthetic Aperture Radar Data: Algorithms and Implementation*. Artech House, Norwood.

El-Mashed, M. G.; Zahran, O.; Dessouky, M. I.; EI-Kordy, M.; Abd EI-Samie, F. E. (2013): Synthetic aperture radar imaging with fractional Fourier transform and channel equalization. *Digital Signal Processing*, vol. 23, no. 1, pp. 151-175.

Fouts, D. J.; Pace, P. E. (2002): A single-chirp false target radar image generator for countering wideband imaging radars. *IEEE Journal of Solid-State Circuits*, vol. 37, no. 6, pp. 751-759.

Hajar, A.; Bijan, Z. (2019): Through-the-multilayered wall imaging using passive synthetic aperture radar. *IEEE Transactions on Geoscience and Remote Sensing*, vol. 57, no. 7, pp. 4181-4191.

He, Q.; Yu, S.; Xu, H.; Liu, J. (2019): A weighted threshold secret sharing scheme for remote sensing images based on Chinese remainder theorem. *Computers, Materials & Continua*, vol. 58, no. 2, pp. 349-361.

Nizar, B.; Stéphane, M. (2019): Unsupervised segmentation of multilook polarimetric synthetic aperture radar images. *IEEE Transactions on Geoscience and Remote Sensing*, vol. 57, no. 8, pp. 6104-6118.

Paul, S.; Pati, U. C. (2020): Automatic optical-to-SAR image registration using a structural descriptor. *IET Image Processing*, vol. 14, no. 1, pp. 62-73.

Qiu, W.; Zhou, J. X.; Fu, Q. (2020): Jointly using low-rank and sparsity priors for sparse inverse synthetic aperture radar imaging. *IEEE Transactions on Image Processing*, vol. 29, pp. 100-115.

Ramona, P.; Nicolas, L.; Grégoire, M.; Guillaume, H.; Rene, G. (2016): Vessel refocusing and velocity estimation on SAR imagery using the fractional Fourier transform. *IEEE Transactions on Geoscience and Remote Sensing*, vol. 54, no. 3, pp. 1670-1684.

Shahzad, G.; Liam, D.; Marina, G.; Bernard, M. (2019): Imaging for a forward scanning automotive synthetic aperture radar. *IEEE Transactions on Aerospace and Electronic Systems*, vol. 55, no. 3, pp. 1420-1434.

Smith, A. M. (1991): A new approach to range-Doppler SAR processing. *International Journal of Remote Sensing*, vol. 12, no. 2, pp. 235-251.

Wang, H. Y.; Jiang, Y. C. (2018): Real-time parameter estimation for SAR moving target based on WVD slice and FrFT. *Electronics Letters*, vol. 54, no. 1, pp. 47-49.

Wang, Z. L.; Wang, Q. (2020): Application of optimal FrFT order for improving the azimuth resolution of range Doppler imaging algorithm. *IET Image Processing*, vol. 14, no. 4, pp. 789-793.

Zhao, X. H.; Deng, B.; Tao, R. (2005): Dimensional normalization in the digital computation of the fractional Fourier transform. *Transactions of Beijing Institute of Technology*, vol. 25, no. 4, pp. 360-364.